crystals

MDPI

Article

Preparation of FeNiCoCrCu Thin Films by Ionized Jet Deposition Method: Determination of Elemental Transfer Coefficients

Jáchym Lis, Jakub Skočdopole, Petr Jaroš, Jiří Čapek, Karel Trojan, Martin Dráb, Monika Kučeráková, Stanislav Vratislav and Ladislav Kalvoda *

Faculty of Nuclear Sciences and Physical Engineering, Czech Technical University in Prague, Břehová 7, 115 19 Prague, Czech Republic; lisjachy@fjfi.cvut.cz (J.L.); jakub.skocdopole@fjfi.cvut.cz (J.S.); jarospe7@fjfi.cvut.cz (P.J.); jiri.capek@fjfi.cvut.cz (J.Č.); karel.trojan@fjfi.cvut.cz (K.T.); martin.drab@fjfi.cvut.cz (M.D.); monika.kucerakova@fjfi.cvut.cz (M.K.); stanislav.vratislav@fjfi.cvut.cz (S.V.)
* Correspondence: ladislav.kalvoda@fjfi.cvut.cz

Abstract: Investigation of high-entropy alloys in form of bulk samples as well as thin films is currently one of the fastest growing areas in the study of metal alloys. In this paper, a bulk sample of FeNiCoCuCr high-entropy alloy ingot with equimolar composition is prepared by the laboratory arc melting method under an argon atmosphere and used as a source target for deposition of thin films on Si (111) single-crystalline substrates using a novel ionized jet deposition method. The morphology, chemical composition, and real crystalline structure of the target and the prepared layers were characterized by scanning electron microscopy, atomic force microscopy, energy-dispersive X-ray spectroscopy, and X-ray and neutron diffraction methods. Transfer coefficients characterizing the mass transport between the target and the grown film were calculated for each of the constituting metallic elements as the ratio of the atomic concentration found in the prepared film divided by its concentration in the deposition target. The dependence of the obtained transfer coefficients on the IJD acceleration voltage is discussed with respect to the main physical and geometric parameters of the deposition process, and their correlations with the cohesive energy of the elements forming the HEA are proposed.

Keywords: high-entropy alloys; FeNiCrCuCo; thin films; ionized jet deposition; SEM; EDXS; AFM; XRD; neutron diffraction; phase composition; elemental transfer coefficients

check for updates

Citation: Lis, J.; Skočdopole, J.; Jaroš, P.; Čapek, J.; Trojan, K.; Dráb, M.; Kučeráková, M.; Vratislav, S.; Kalvoda, L. Preparation of FeNiCoCrCu Thin Films by Ionized Jet Deposition Method: Determination of Elemental Transfer Coefficients. *Crystals* **2024**, *14*, 263. https://doi.org/10.3390/cryst14030263

Academic Editors: Zaoli Zhang and Alessandra Toncelli

Received: 26 December 2023
Revised: 23 February 2024
Accepted: 1 March 2024
Published: 7 March 2024

Copyright: © 2024 by the authors. Licensee MDPI, Basel, Switzerland. This article is an open access article distributed under the terms and conditions of the Creative Commons Attribution (CC BY) license (https://creativecommons.org/licenses/by/4.0/).

1. Introduction

Coatings and thin films prepared from high-entropy alloys (HEAs) attract significant attention due to their ability to bypass the relatively poor formability of HEAs and combine/merge their unique physical properties, such as enhanced hardness and Young's modulus, reduced wear rate, superior corrosion resistance, excellent temperature and oxidation resistance, excellent thermal stability of their mechanical properties, and strong diffusion retardation [1,2]; the base workpieces are shaped and manufactured by standard technologies.

Among the different HEAs tested, an important place belongs to HEA with a composition of FeNiCrCoCu, which shows excellent ductility [3], wear resistance, high hardness, and corrosion resistance [4]. A face-centered cubic (FCC) structure consisting of one or two phases differing in the lattice parameter is reported for equimolar FeNiCrCoCu [3,5]. However, the phase composition is found to be sensitive to addition of even small amount of Al or Ti [3,6,7], and shows changes as a result of ageing and re-crystallization processes [5,8]. Such behavior suggests that there is likely only a small difference between the contributions of the configuration entropy and the mixing enthalpy to the total Gibbs energy of this metallic system.

Currently, a range of deposition techniques are routinely used in the preparation of thin films and protective coatings [9,10]. Many of these methods have also been successfully applied in the preparation of thin films formed of HEAs. In particular, regarding the FeNiCrCo-based HEA system investigated here, the already reported deposition techniques applied include cold-spraying [11], electrochemical deposition [12], laser cladding [13], direct current [14], radio frequency [15], magnetron sputtering, and plasma cladding [16]. Continuing in our efforts to prepare HEA thin films by ionized jet deposition (IJD) [17], this paper aims to extend the list of the above-mentioned methods to include this novel thin film deposition technique.

The IJD method belongs to the group of physical vapor deposition (PVD) techniques. The IJD deposition head is placed in a vacuum chamber and provides a pulsing electron beam guided and accelerated by the applied pulsing high voltage (U) through a conductive channel (a plasma duct formed by the ionized working gas) towards the source target. The plasma plume arising from the emission of the target material is then directed towards the selected substrate where it condenses and forms the growing thin film. For a more detailed description of the physical mechanisms that play a major role in the function of IJD deposition head, see our previous reports [17,18].

The nature and kinetics of interaction processes between the primary electronic beam accelerated by the IJD head and the deposition target then have a key impact on the elemental content in the target plasma plume. In this respect, the IJD method has much in common with other deposition techniques, such as pulse laser deposition (PLD), magnetron sputtering (MS), and channel spark deposition (CSD). Depending on the particular type and parameters of the primary beam used (photons, ions, and electrons in the case of PLD, MS, and CSD/IJD, respectively), these methods combine two different physical mechanisms for releasing material from the deposition target in varying proportions. As described for PLD by Venkatesan et al. [19], the two mentioned routes consist of the (desired) ablation process acceptably preserving the stoichiometric composition of the target and the (undesired) non-stoichiometric thermal evaporation process.

Comparing PLD and IJD methods, the difference in the type of the primary energetic beam used to invoke the required target material ablation leads to the different physical interaction processes involved. Unlike PLD, the IJD method is suitable for the deposition of optically non-absorbing materials, and the primary beam is not disturbed by its absorption in the plasma plume emitted from the target. The latter property allows for the application of high deposition frequencies of the pulsing IJD source. The other practical assets characterizing the IJD method include high flexibility in selection of the material to be deposited; a well-defined, voltage-tunable stoichiometry transfer ratio between the target and the growing layer; a generally low thermal load of the deposited material; and the possibility of reactive deposition of, e.g., nitrides or oxides of the source material by selecting the proper working gas (e.g., N_2, O_2). Unlike the magnetron sputtering source, then, an easy up-scalability of the IJD deposition system is possible due to the compact construction and robustness of the IJD head and the well-defined directional character of its emission, allowing for the possibility of simply installing multiple deposition heads in the deposition chamber, connecting the heads to a common high-voltage source, and operating at phase-shifted shot frequencies.

In this paper, we present the results obtained in the preparation and characterization of the bulk material (used as the deposition target) and the IJD-deposited thin films composed of FeNiCrCoCu HEA. The morphology, chemical composition, and real crystalline structure of the bulk sample and the prepared films are then correlated with the key IJD deposition parameters, and the elemental transfer coefficients (T) are calculated, depending on the applied IJD head voltage. The transfer coefficients provide elementally specific quantitative measure of the mass transfer process between the target bulk and the growing layer. The obtained results are then compared with the results of previous IJD experiments and other deposition techniques.

2. Materials and Methods

An Edmund Bühler AM200 arc melting furnace (AMF) was used in the preparation of the FeNiCrCoCu HEA ingot. In the first step, the selected initial elemental powders (Sigma-Aldrich s.r.o., Prague, Czech Republic, 99.99% trace metals basis) were mixed together in an equimolar ratio to give a total mass of 10 g. The mixture was then exposed to the pressure molding (10 MPa) to obtain a compact pellet, and the latter one repeatedly arc-melted under an inert gas atmosphere (Ar, gas purity 99.999, supplied by Linde Technoplyn s.r.o., Prague, Czech Republic). The final disc-shaped mold was then used as the target in IJD preparation of thin FeNiCrCoCu HEA films.

The IJD deposition system JetDep 100 installed in the laboratories of the Department of Solid State Engineering, Faculty of Nuclear Science and Physical Engineering of the Czech Technical University in Prague was used in the preparation of four samples (S1–S4) of thin films composed of FeNiCrCoCu HEA, deposited on Si (111) single-crystalline substrates, with the IJD head voltage gradually set to 16, 17, 18, and 19 kV for the S1, S2, S3, and S4 samples, respectively. This particular voltage range was chosen in order to reduce the thermal/energetic exposition of the target and to test the effect of the accelerating voltage level on the nature of the interaction of the primary electron beam with the target and influence of this interaction on the elemental transfer between the target and the growing layer.

The other main IJD deposition parameters common for all prepared samples were as follows: the repetition rate of the IJD source was fixed at 20 Hz, the distance between the target and the substrate set to 100 mm, the distance between the IJD source and the target set within 2.5–4.0 mm for the individual depositions (the difference arising due to the unevenness of the target surface), and the electron beam pulse duration and power density adjusted to 200 ns and 14 MW/cm^2, respectively. The mean primary electron beam spot diameter on the target amounted to 1 mm. The substrate temperature and the film deposition time were set to 300 K and 120 min, respectively. A gas mixture of Ar + 6 vol. % H_2 was used as the IJD working gas (purity 99.999, provided by Linde Technoplyn, s.r.o., Prague, Czech Republic) in order to ensure the desired environment for the film growth, reducing the possible metal oxide formation rate. The initial pressure before deposition and the working pressure were set in the range of (3.0–4.1) $\times$ 10^{-5} mbar and (5.2–7.2) $\times$ 10^{-4} mbar, respectively.

Scanning electron microscopy (SEM), energy-dispersive X-ray spectroscopy (EDXS), atomic force microscopy (AFM), X-ray diffraction (XRD), and neutron diffraction (ND) methods were used in the characterization of the prepared FeNiCrCoCu HEA target and the deposited thin film samples. The SEM and EDXS measurements were performed with a MAIA3 scanning electron microscope (Tescan Group a.s, Brno, Czech Republic). The SEM pictures were collected using a secondary electrons detector, with the primary electron beam of energy 10–15 keV. The EDXS spectra were recorded with the X-Max150 analyzer and a 20 mm^2 silicon drift detector (Oxford Instruments Inc., Abingdon, UK). The obtained EDXS chemical composition data were then analyzed using AZtecEnergy 2.1 evaluation software. An atomic force microscope LiteScope (NenoVision s.r.o., Brno, Czech Republic) equipped with the Akyiama probe was used to characterize the surface topology of the prepared films. The XRD patterns used in the crystallographic phase composition analysis of the prepared films were recorded on an X'Pert PRO MPD diffractometer (Malvern Panalytical B.V., Almelo, The Netherlands) equipped with a position-sensitive X'Cellerator detector using CoKα filtered radiation. The obtained XRD data were evaluated with the aid of the HighScore Plus program and the Powder Diffraction File (PDF) database [20,21]. The crystallographic phase composition of the FeNiCrCoCu HEA bulk target was obtained from the ND patterns collected on the KSN-2 powder diffractometer installed at the HK-2 horizontal channel of the research nuclear reactor LVR-15 (Nuclear Research Institute Řež, plc., Řež, Czech Republic). The KSN-2 provides the utmost interplanar distance (d) resolution value of $\Delta d/d = 0.007$ in the range of d between 1.0 and 0.1 nm. A parallel collimated primary beam of monochromatic neutrons with the mean wavelength $\lambda = 0.1362$ nm was used, obtained by reflection from the single-crystal Cu (200) monochromator and collimated

by three consecutive Soller slits collimators. The obtained ND patterns were evaluated with the program GSAS [22,23].

The process of elemental transfer from the IJD deposition target to the growing film was quantitatively characterized by the transport coefficient (T) calculated for each metallic element present in the FeNiCrCoCu HEA following the formula

$$T = C_F / C_T \quad (1)$$

Here, C_F and C_T are the mean atomic concentration of the selected element in the resulting film and the used deposition target, respectively.

3. Results and Discussion

3.1. Deposition Target

The SEM micrograph of the target ingot surface (Figure 1a) shows a highly porous, coral-like structure resulting from the arc melting process used in the target casting. The EDXS elemental maps confirm a uniform distribution of the constituting metallic elements over the target surface (Figure 1b–f). The recorded EDXS spectra also show the presence of oxygen and carbon contamination, with the surface distributions of the latter impurities showing a higher degree of surface unevenness compared to the distribution of the constituting metals (Figure 1g,h). The composition data obtained by EDXS are summarized in Table 1.

Let us note that a reliable, exact determination of the real oxygen and carbon contents in the target bulk itself is, however, difficult with regard to the possible contamination of the target surface and the EDXS analytic chamber by these elements; we must also take into account the proximity of the OKα1 and CrKα1 emission line energies. For the latter reason, the same caution applies for the concentration data obtained for Cr.

The results of ND measurements are summarized in Table 2. The bulk crystallographic phase composition of the target is found to contain two phases: a dominant austenitic phase (face-centered cubic (FCC), space group $Fm\bar{3}m$) and a small amount of additional martenzitic phase (hexagonal close-packed (HCP), space group $P6_3/mmc$). No presence of a ferritic phase (body-centered cubic (BCC), space group $Im\bar{3}m$) is found. The absence of BCC phase as well as the observed lattice parameter value of the FCC phase is conformal with the published results obtained for bulk FeNiCoCrCu HEA samples in [3,5] where, however, only a single FCC phase was observed. Our sample thus deviates slightly from the perfect state corresponding to an HEA formed by a single FCC solid solution.

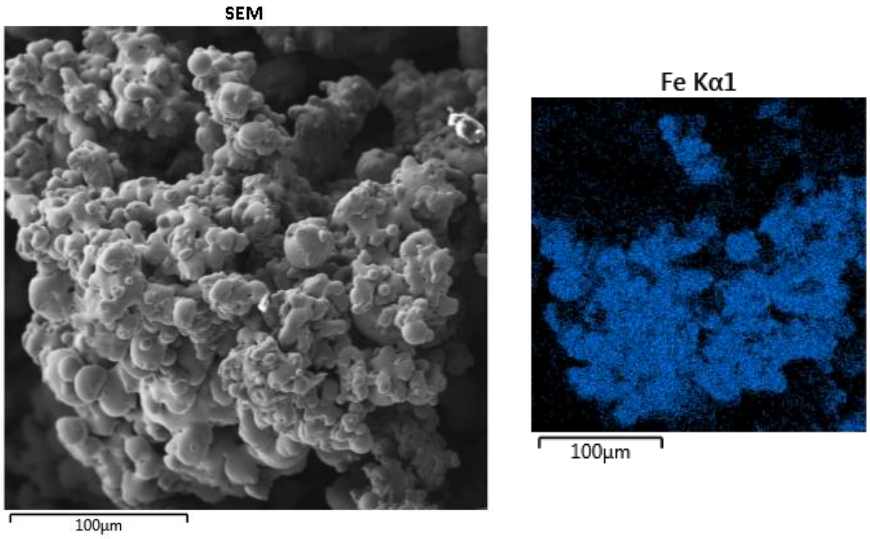

(**a**) (**b**)

Figure 1. *Cont.*

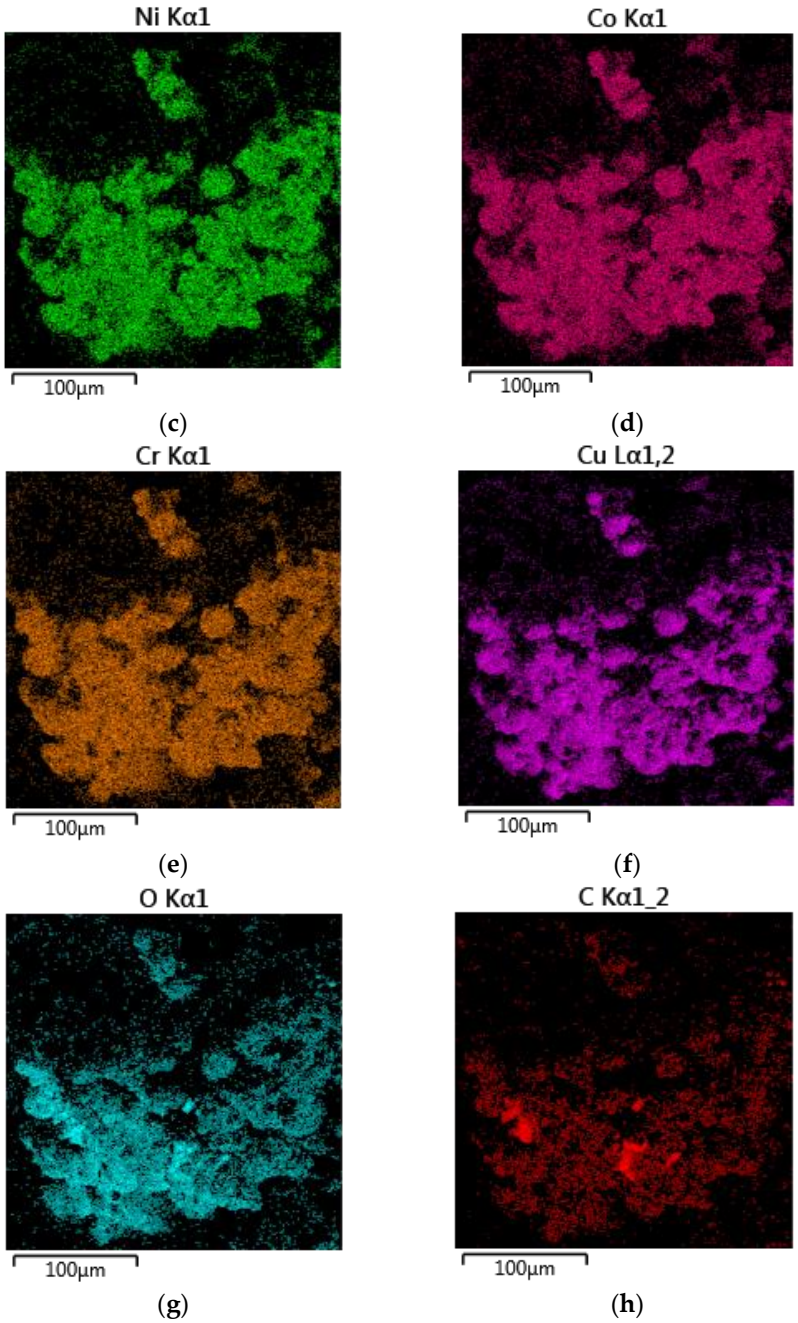

Figure 1. SEM micrograph (**a**) and EDXS elemental maps recorded from the same place (**b**–**h**) of the as-prepared FeNiCoCrCu ingot; magnification 1000; 15 kV primary electron beam. SEM pictures recorded using secondary electrons; the element and X-ray emission line symbols are indicated for each of the EDXS maps shown.

Table 1. Elemental atomic concentrations obtained by EDXS for the raw FeNiCoCrCu ingot.

Element	Fe	Ni	Co	Cr	Cu	O	C
Concentration (at. %)	16.7 ± 0.1	16.6 ± 0.1	18.5 ± 0.1	10.4 ± 0.1	13.8 ± 0.1	5.4 ± 0.1	18.6 ± 0.2

The texture index (scaled between 1 and infinity and calculated by GSAS [22] as the quantitative measure of the orientation anisotropy of crystalline grains forming the tested polycrystal) is found to be remarkably higher for the minority HCP phase. However, given the small relative proportion of this phase, the above result must be taken with caution.

The results obtained for the bulk FeNiCoCrCu HEA ingot (with a homogenous elemental distribution over the ingot surface and a phase composition dominated by FCC phase) confirm that the material is well suited for use as a deposition target despite the undesirable contamination with elements O and C. Achieving higher elemental and phase purity of the target will be one of the aims of our further research on the subject.

Table 2. Real crystallographic structure parameters obtained from the GSAS fit to the experimental ND patterns of bulk FeNiCrCoCu HEA ingot; the values of R-factor and χ^2 relate to the Rietveld fit of the ND patterns.

Phase	Space Group	a (nm)	c (nm)	Relative Phase Content (wt. %)	Texture Index	R-Factor (%)	χ^2
FCC	$Fm\bar{3}m$	0.3593	-	90.2	3.11	8.8	1.74
HCP	$P6_3/mmc$	0.2529	0.4156	9.8	20.4	8.8	1.74

3.2. Thin Films

SEM and AFM micrographs of the thin film samples S1–S4 show all a similar surface topology character containing frequent spherical surface irregularities (bulges) with a characteristic dimension in the range of hundreds of nanometers (the results obtained for sample S2 are shown in Figure 2a,b as an example). The presence of bulges can be suppressed by the fine-tuning of the IJD acceleration voltage and the target-to-substrate distance.

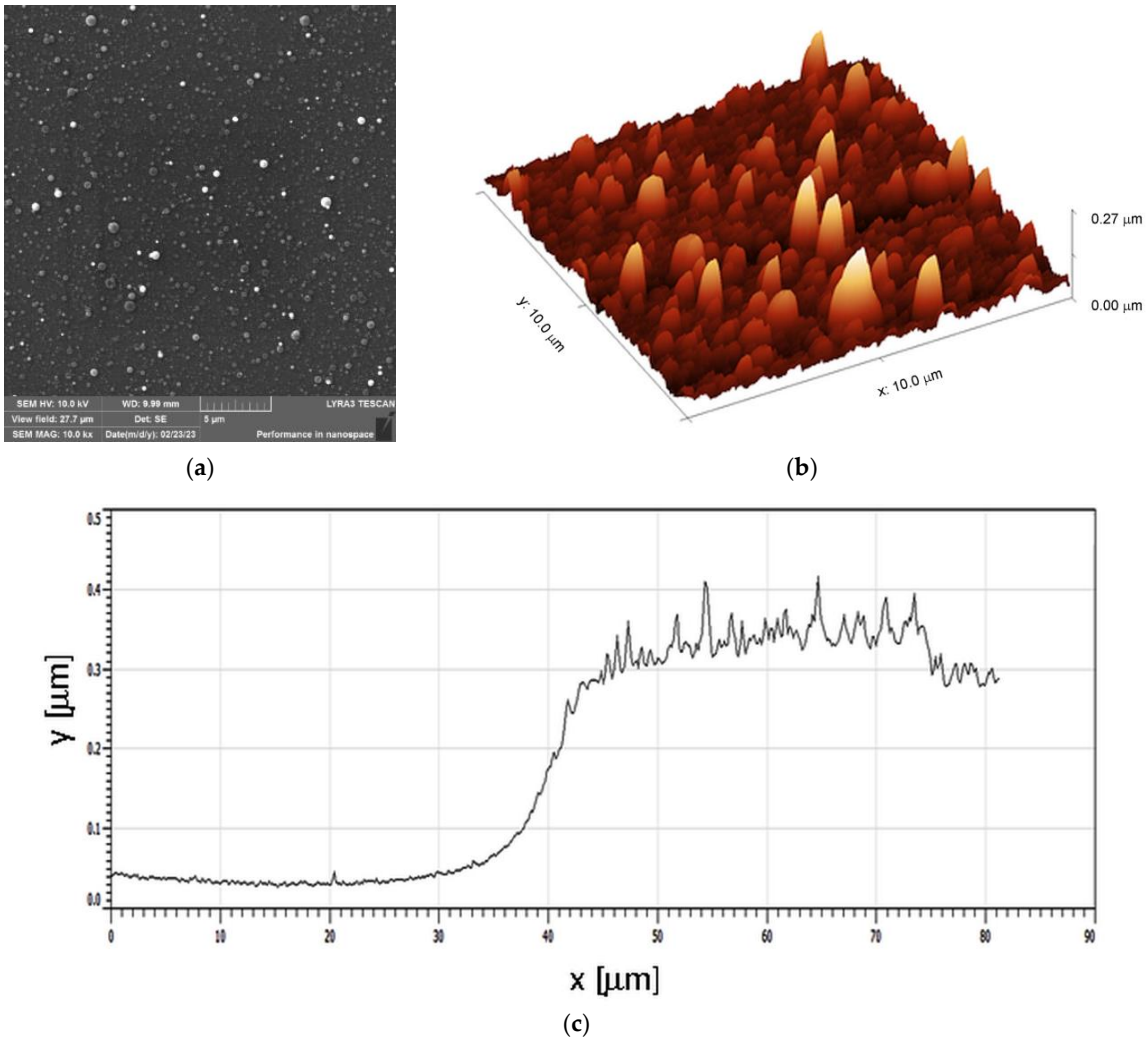

(**a**) (**b**)

(**c**)

Figure 2. Sample S2: SEM micrograph (**a**), AFM surface 3D map (**b**), and AFM scan profile over the layer edge (**c**).

From the AFM scans performed over edge of the prepared films, their thickness is obtained (Figure 2c). The mean growth speed values can be then calculated for all the prepared film samples as the ratio of thickness obtained from AFM measurements to the total deposition time. The obtained results are summarized in Table 3.

Table 3. Thickness and mean growth rate obtained for the prepared film samples S1–S4. Values of deposition parameters with a significant influence on these characteristics are also given.

Sample	S1	S2	S3	S4
IJD voltage (kV)	16	17	18	19
Working pressure (10^{-4} mbar)	7.0	6.8	7.2	5.2
Head-to-target distance (mm)	3.0	3.0	4.0	2.5
Resulting film thickness (nm)	347 ± 6	363 ± 6	263 ± 26	383 ± 17
Mean growth rate (nm/min)	2.89 ± 0.05	3.02 ± 0.05	2.19 ± 0.22	3.20 ± 0.14

The decrease in the growth rate observed for sample S3 compared to the other samples can be attributed to the combined effect of the higher working gas pressure and the larger distance between the IJD head and the target which was used for this sample.

The XRD phase analysis of the prepared layers again suggests the presence of two crystallographic phases, FCC and HCP, in agreement with the situation observed for the deposition target. Due to the low thickness of the prepared layers, however, the recorded XRD patterns contain only several broad diffraction maxima (an example for the sample S3 is given in Figure 3), making a more detailed quantitative phase analysis impossible.

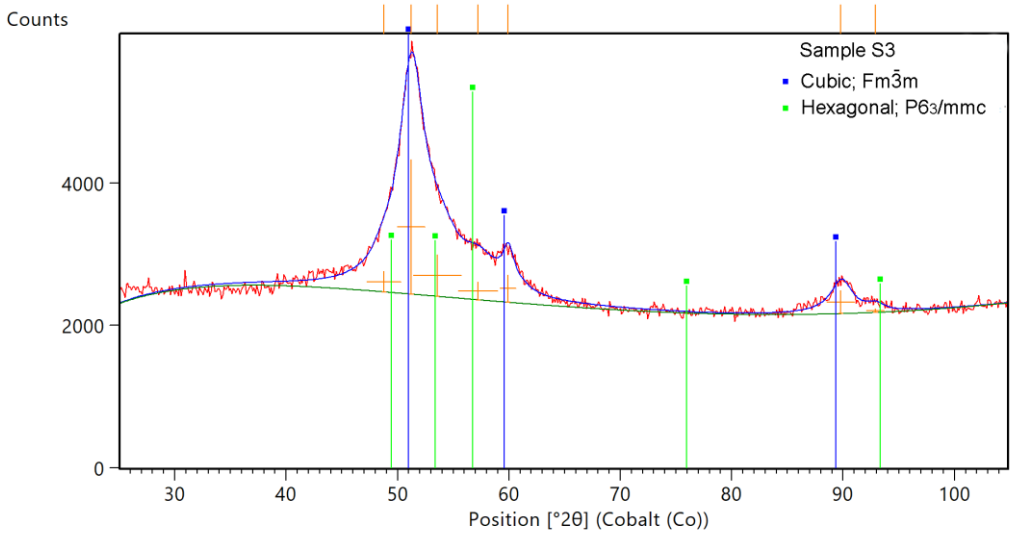

Figure 3. XRD patterns observed for the sample S3; the angular positions and relative intensities of the diffraction lines, corresponding to the crystallographic phases indicated in the legend, are marked by the matching color lines and points, respectively; the orange lines and crosses mark then the respective actual positions and intensities of the reflections fitted to the experimental diffraction profile.

The mean elemental atomic concentrations measured by EDXS for all prepared film samples are summarized in Table 4. The concentration values were obtained as an average of the concentrations measured at several randomly selected locations near the center of the film. For all thin film samples, the content of O and C impurities is higher compared to the target, with the increase roughly following the working gas pressure and/or head-to-target distance settings (cf. Table 3). An inverse proportionality with respect to the former deposition parameters has already been observed for the growth rate values; thus, the setting of these parameters needs to be complexly optimized.

Table 4. Elemental concentration (at. %) obtained by EDXS for the prepared thin film samples S1–S4.

Element	S1	S2	S3	S4
Cr	7.4 ± 0.2	7.1 ± 0.2	7.5 ± 0.2	8.1 ± 0.2
Fe	13.0 ± 0.3	15.4 ± 0.3	13.7 ± 0.2	15.0 ± 0.3
Co	16.0 ± 0.4	17.1 ± 0.4	16.0 ± 0.3	18.0 ± 0.4
Ni	16.6 ± 0.5	17.5 ± 0.5	16.6 ± 0.5	18.4 ± 0.5
Cu	17.0 ± 0.2	16.5 ± 0.2	15.9 ± 0.2	17.4 ± 0.2
O	22.5 ± 0.3	17.2 ± 0.3	20.6 ± 0.3	12.7 ± 0.3
C	7.6 ± 0.4	10.1 ± 0.4	9.8 ± 0.3	10.5 ± 0.4

3.3. Transfer Coefficients

The calculation of transfer coefficients was carried out in accordance with Formula (1) using the relative concentrations, with no content of non-metallic elements (O, C) considered (Table 5). The values shown here slightly differ from the values given in Table 1 not only because the oxygen and carbon content is neglected but also because a different measurement procedure was applied. For the target already used in IJD deposition, the values were obtained as the mean atomic composition averaged over two different positions on the target surface: at the edge of a surface hollow created by the impact of the primary IJD electron beam and at a position far away from that hollow. Values of the elemental transfer coefficients calculated for all prepared films and constituting metallic elements are shown in Figure 4. The obtained results demonstrate the elemental dependence of T on the particular IJD-accelerating voltage applied.

Table 5. Relative atomic concentrations of the constituting metallic elements only obtained by the EDXS method for the prepared thin film samples S1, S2, S3, and S4, as well as the deposition target used.

Element	Atomic Number	S1	S2	S3	S4	Target
Cr	24	10.5 ± 0.2	9.7 ± 0.2	10.8 ± 0.2	10.5 ± 0.2	13.7 ± 0.1
Fe	26	18.5 ± 0.4	19.9 ± 0.4	19.7 ± 0.3	19.5 ± 0.3	21.9 ± 0.1
Co	27	22.9 ± 0.4	23.6 ± 0.4	22.9 ± 0.4	23.4 ± 0.4	24.4 ± 0.1
Ni	28	23.8 ± 0.5	24.0 ± 0.5	23.8 ± 0.5	23.9 ± 0.5	21.8 ± 0.1
Cu	29	24.3 ± 0.3	22.7 ± 0.3	22.8 ± 0.3	22.7 ± 0.3	18.2 ± 0.1

Apparently, for the given element, the mean T value averaged over the applied IJD voltage range increases with the atomic number of the element. A qualitatively similar result was already obtained in our former study [17] dealing with IJD deposition of HfNbTiTaZr HEA films, which was performed with the IJD voltage varying over a voltage range of 16–22 kV. Contrary to the HfNbTiTaZr HEA films, however, where stabilization of the observed T values occurred for IJD voltages equal or exceeding 20 kV [17], only a weak dependence of T on the IJD acceleration voltage is observed for FeNiCrCoCu films within the applied voltage range of 16–19 kV. The latter finding confirms that for all the applied voltage levels, the primary IJD electron beam energy already reaches/exceeds the ablation threshold of the FeNiCrCoCu target [24]. Here, we recall that the primary IJD electron beam energy, proportional to the adjusted IJD head acceleration voltage, controls the ablation conditions of the given target together with the thermal diffusion length.

In a review presented by Schou [25], dealing with PLD method, the complex processes taking place during ablation of the target material are discussed (in this case, a high-temperature superconductor exposed to a pulsing energetic laser beam); these processes then affect the subsequent stoichiometric mass transfer from the target to the growing film. Several key steps in the whole transfer are identified and evaluated, and they also remain in force for the IJD method. These include primary beam energy absorption in the target bulk, fast initial 1-D expansion of the formed plasma plume, subsequent 3-D adiabatic plasma expansion combined with the slowing down of the plasma plume under the influence of the

background gases present in the deposition chamber, and finally, processes accompanying the mass accommodation/condensation on the substrate and growth of the resulting film.

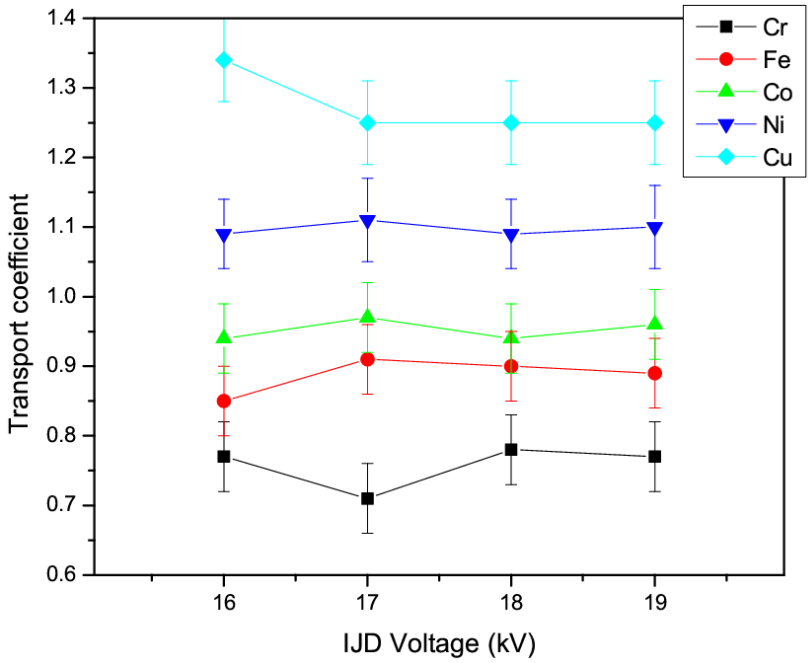

Figure 4. Transport coefficients of the metallic elements constituting the tested HEA, shown to depend on the applied IJD voltage; the error bars indicate the corresponding ESDs.

Within the first step, the ablation yield is found to be controlled by the cohesive energy value of the target material. Some correlation is found between the cohesive energy and the melting point values of the elements that the target is composed of. However, we also observed a non-negligible influence of concurrent non-linear and non-additive multi-elemental interactions [25]. This must be considered in cases of complex multi-component materials such as HEAs. Moreover, the situation might be further complicated by a possible spatial non-uniformity of the primary beam interaction with the target (leading to local fluctuations between the pure ablation and the pure thermal evaporation limits), which can be caused, e.g., by a non-uniform spatial distribution of the primary beam power, the influence of anisotropic heat dissipation in the target, and the initiation of possible structural changes in the target (such as elemental surface segregation and/or elementally selective surface depletion) after the prolonged action of the primary beam, etc.

A detailed analysis of all these processes is beyond the scope of this article due to their high level of complexity. In the following discussion, we restrict ourselves to the initial phase, the release of mass from the target, which we believe has the greatest influence on the value of the transfer coefficients obtained here. The observed correlation between the transfer coefficients and the atomic numbers of the elements effectively demonstrates one important and characteristic feature of the HEAs (or the alloy studied in this paper, which was dominated by HEA solid solution), namely their special elemental formulation which includes elements with similar atomic mass and a high-level mutual miscibility, resulting then in the dominant presence of a single solid solution phase. This means they conform with small, mutually similar, and preferentially matching pairwise elemental mixing enthalpy values [26]. The latter characteristic then causes the ablation yield to be dominated by the atomic mass of the involved atoms (and to a much lesser extent by their mutual interactions). The higher voltage threshold observed for the onset of the ablation-controlled deposition mode in the case of HfNbTiTaZr HEA films [17] (compared to the FeNiCrCoCu HEA films studied in this work) is thus in line with (on average) the higher cohesive energy of the elements present in the HfNbTiTaZr HEA as compared with the FeNiCrCoCu alloy [27].

4. Conclusions

An FeNiCoCrCu HEA ingot was prepared by the arc melting method, showing a uniform spatial distribution of the constituting metallic elements and real crystalline structure dominated by the austenitic FCC phase, with a small amount of highly textured HCP phase. The ingot was then used as a target in the preparation of thin films according to the IJD method. The films were deposited with an IJD acceleration voltage gradually increasing in the range between 16 and 19 kV. All four prepared film samples showed an uneven surface morphology containing spherical bulges hundreds of nanometers in diameter. An increase in the concentration of oxygen and carbon impurities in the films compared to the deposition target was also observed, correlated with the instrumental settings of the deposition process. A fine adjustment of the acceleration voltage combined with optimization of the geometric parameters and the working gas flow will be necessary in order to improve these undesirable features.

Transfer coefficients characterizing elemental transport between the target and the prepared films were calculated based on the obtained relative concentrations of the five constituting metallic elements. The values of the transfer coefficient were found to be stable within the whole of the applied IJD accelerating voltage range, indicating the dominant influence of the ablation interaction mechanism between the electron beam emitted by the IJD head and the target. The relative magnitude of the transport coefficients obtained for individual elements was then found to be proportional to the atomic number of the given element. An explanation is proposed, interpreting this finding as a direct consequence of the special elemental mixing properties characteristic of HEA solid solutions in general. Verification of this hypothesis will be the subject of our further research.

Author Contributions: Conceptualization, J.L., P.J., J.S., J.Č., K.T., S.V. and L.K.; methodology, J.S., J.Č. and S.V.; software, M.D., J.L. and J.S.; validation, J.S., J.Č., K.T., M.K. and L.K.; formal analysis, J.L., J.S. and S.V.; investigation, J.L., J.S., P.J., J.Č., K.T., M.K. and S.V.; resources, J.L., J.S. and L.K.; data curation, J.L., J.S., J.Č., K.T., M.K., M.D. and S.V.; writing—original draft preparation, J.S., M.K., J.Č. and L.K.; writing—review and editing, L.K.; visualization, J.L., J.S., J.Č. and K.T.; supervision, J.S. and L.K.; project administration, L.K.; funding acquisition, L.K. All authors have read and agreed to the published version of the manuscript.

Funding: This research was funded by the Czech Science Foundation grant GA21-05259S, and the Grant Agency of the Czech Technical University in Prague, grant No. SGS22/183/OHK4/3T/14.

Data Availability Statement: Data are available from the authors upon personal request.

Conflicts of Interest: The authors declare no conflicts of interest. The funders had no role in the design of the study; in the collection, analyses, or interpretation of data; in the writing of the manuscript or in the decision to publish the results.

References

1. Yan, X.H.; Li, J.S.; Zhang, W.R.; Zhang, Y. A brief review of high-entropy films. *Mater. Chem. Phys.* **2018**, *210*, 12–19. [CrossRef]
2. Li, W.; Liu, P.; Liaw, P.K. Microstructures and properties of high-entropy alloy films and coatings: A review. *Mater. Res. Lett.* **2018**, *6*, 199–229. [CrossRef]
3. Wang, X.; Zhang, Y.; Qiao, Y.; Chen, G. Novel microstructure and properties of multicomponent CoCrCuFeNiTix alloys. *Intermetallics* **2007**, *15*, 357–362. [CrossRef]
4. Li, J.; Dong, L.; Dong, X.; Zhao, W.; Liu, J.; Xiong, J.; Xu, C. Study on wear behavior of FeNiCrCoCu high entropy alloy coating on Cu substrate based on molecular dynamics. *Appl. Surf. Sci.* **2021**, *570*, 151236. [CrossRef]
5. Park, N.; Watanabe, I.; Terada, D.; Yokoyama, Y.; Liaw, P.K.; Tsuji, N. Recrystallization Behavior of CoCrCuFeNi High-Entropy Alloy. *Metall. Mater. Trans. A* **2015**, *46*, 1481. [CrossRef]
6. Jones, N.G.; Frezza, A.; Stone, H.J. Phase equilibria of an Al0.5CrFeCoNiCu High Entropy Alloy. *Mater. Sci. Eng.* **2014**, *A615*, 214–221. [CrossRef]
7. Li, B.; Peng, K.; Hu, A.; Zhou, L.; Zhu, J.; Li, D. Structure and properties of FeCoNiCrCu0.5Alx high-entropy alloy. *Trans. Nonferrous Met. Soc. China* **2013**, *23*, 735–741. [CrossRef]
8. Thangaraju, S.; Bouzy, E.; Hazotte, A. Phase Stability of a Mechanically Alloyed CoCrCuFeNi High Entropy Alloy. *Adv. Eng. Mater.* **2017**, *19*, 1700095. [CrossRef]

9. Chaudhari, M.N.; Ahirrao, R.B.; Bagul, S.D. Thin film Deposition Methods: A Critical Review. *IJRASET* **2021**, *9*, 5215–5232. [CrossRef]
10. Budida, J.; Srinivasan, K. Review of thin film deposition and techniques. *Mater. Today Proc.* **2023**, *92*, 1030–1033. [CrossRef]
11. Yin, S.; Li, W.; Song, B.; Yan, X.; Kuang, M.; Xu, Y.; Wen, K.; Lupoi, R. Deposition of FeCoNiCrMn high entropy alloy (HEA) coating via cold spraying. *J. Mater. Sci. Technol.* **2019**, *35*, 1003–1007. [CrossRef]
12. Aliyu, A.; Rekha, M.Y.; Srivastava, C. Microstructure-electrochemical property correlation in electrodeposited CuFeNiCoCr high-entropy alloy graphene oxide composite coatings. *Philos. Mag.* **2019**, *99*, 718–735. [CrossRef]
13. Jin, G.; Cai, Z.; Guan, Y.; Cui, X.; Liu, Z.; Li, Y.; Dong, M.; Zhang, D. High temperature wear performance of laser-cladded FeNiCoAlCu high-entropy alloy coating. *Appl. Surf. Sci.* **2018**, *445*, 113–122. [CrossRef]
14. Sha, C.; Zhou, Z.; Xie, Z. Paul Munroe: FeMnNiCoCr-based high entropy alloy coatings: Effect of nitrogen additions on microstructural development, mechanical properties and tribological performance. *Appl. Surf. Sci.* **2020**, *507*, 145101. [CrossRef]
15. Pu, G.; Lin, L.; Ang, R.; Zhang, K.; Liu, B.; Liu, B.; Peng, T.; Liu, S.; Li, Q. Outstanding radiation tolerance and mechanical behavior in ultra-fine nanocrystalline Al1.5CoCrFeNi high entropy alloy films under He ion irradiation. *Appl. Surf. Sci.* **2020**, *516*, 145129. [CrossRef]
16. Peng, Y.; Zhang, W.; Li, T.; Zhang, M.; Liu, B.; Liu, Y.; Wang, L.; Hu, S. Effect of WC content on microstructures and mechanical properties of FeCoCrNi high-entropy alloy/WC composite coatings by plasma cladding. *Surf. Coat. Technol.* **2020**, *385*, 125326. [CrossRef]
17. Skočdopole, J.; Čech, J.; Čapek, J.; Trojan, K.; Kalvoda, L. Preparation of HfNbTiTaZr Thin Films by Ionized Jet Deposition Method. *Crystals* **2023**, *13*, 580. [CrossRef]
18. Skočdopole, J.; Kalvoda, L.; Nozar, P.; Netopilík, M. Preparation of polymeric coatings by ionized jet deposition method. *Chem. Pap.* **2018**, *72*, 1735–1739. [CrossRef]
19. Venkatesan, T.; Wu, X.D.; Inam, A.; Wachtman, J.B. Observation of two dis-tinct components during pulsed laser deposition of high T c superconducting films. *Appl. Phys. Lett.* **1988**, *52*, 1193–1195. [CrossRef]
20. Degen, T.; Sadki, M.; Bron, E.; König, U.; Nénert, G. The HighScore suite. *Powder Diffr.* **2014**, *29*, S13–S18. [CrossRef]
21. Gates-Rector, S.; Blanton, T. The Powder Diffraction File: A Quality Materials Characterization Database. *Powder Diffr.* **2019**, *34*, 352–360. [CrossRef]
22. Toby, B.H. EXPGUI, a graphical user interface for GSAS. *J. Appl. Crystallogr.* **2001**, *34*, 210–213. [CrossRef]
23. Larson, A.C.; Von Dreele, R.B. General Structure Analysis System (GSAS). *Los Alamos Natl. Lab. Rep. LAUR* **2004**, *748*, 86–748.
24. Strikovski, M.; Harshavardhan, K.S. Parameters that control pulsed electron beam ablation of materials and film deposition processes. *Appl. Phys. Lett.* **2003**, *82*, 853–855. [CrossRef]
25. Schou, J. Physical aspects of the pulsed laser deposition technique: The stoichiometric transfer of material from target to film. *Appl. Surf. Sci.* **2009**, *255*, 5191–5198. [CrossRef]
26. Miracle, D.B.; Senkov, O.N. A critical review of high entropy alloys and related concepts. *Acta Mater.* **2017**, *122*, 448–511. [CrossRef]
27. Kittel, C. *Introduction to Solid State Physics*, 8th ed.; John Wiley & Sons, Inc.: Hoboken, NJ, USA, 2005; p. 50.

Disclaimer/Publisher's Note: The statements, opinions and data contained in all publications are solely those of the individual author(s) and contributor(s) and not of MDPI and/or the editor(s). MDPI and/or the editor(s) disclaim responsibility for any injury to people or property resulting from any ideas, methods, instructions or products referred to in the content.